ASME Journal of Offshore Mechanics and Arctic Engineering
Online journal at:
https://asmedigitalcollection.asme.org/offshoremechanics

**Aris G. Stamou**
Department of Mechanical Engineering,
University of Thessaly,
Volos 38334, Greece
e-mail: aristamou@uth.gr

**Ilias Gavriilidis**
Department of Mechanical Engineering,
University of Thessaly,
Volos 38334, Greece
e-mail: ilgavrii@uth.gr

**Spyros A. Karamanos**[1]
Department of Mechanical Engineering,
University of Thessaly,
Volos 38334, Greece
e-mail: skara@mie.uth.gr

**Christos Palagas**
Corinth Pipeworks S.A.,
Thisvi 32010, Greece
e-mail: cpalagas@cpw.gr

**Doug Swanek**
C-FER Technologies,
Edmonton, AB T6N 1H2, Canada
e-mail: d.swanek@cfertech.com

# Collapse Performance of High-Frequency Welded Steel Pipes for Offshore Applications: Experiments and Numerical Simulations

*The present article investigates the collapse performance of steel pipes fabricated by the high-frequency welding (HFW) method. Two 16-in. outer diameter HFW line pipe specimens are subjected to full-scale external pressure testing in order to determine their collapse pressure and propagation pressure. Prior to testing, one of the pipes has been externally coated, which introduced a mild heat treatment to the pipe, while the other pipe remained intact (noncoated). The full-scale test procedure is modeled with a computationally efficient finite element methodology, which accounts for the actual geometry and material properties, and employs a simple and efficient technique for simulating pipe collapse and buckle propagation. The numerical results compare very well with the full-scale experimental results, in terms of the values of collapse and propagation pressure, the collapsed shape and history of local strains at critical locations. Both experimental and numerical results show a very good performance of HFW pipes against collapse, indicating that those pipes can be strong candidates for offshore applications. The analytical procedure for predicting the collapse and propagation pressure in DNV-ST-F101 is also evaluated and shows that its conservative predictions are improved if an appropriate value of fabrication factor is used.* [DOI: 10.1115/1.4071998]

*Keywords: offshore pipeline, pipe collapse, propagating instability, structural stability, full-scale test, cold-formed pipe*

## 1 Introduction

The installation of offshore pipelines in deep-water environments presents significant engineering challenges, primarily due to the presence of high hydrostatic pressure. Under these conditions, pipelines are vulnerable to structural failure in the form of collapse, which is a special form of structural instability. It is typically manifested as localized flattening of the pipe cross section, and upon its formation, it may propagate along the pipeline [1–3]. Collapse occurs when the applied external pressure exceeds the critical buckling pressure ($P_c$), the ultimate (maximum) pressure level, also referred to as "collapse pressure," that the pipe is capable to sustain. The collapse pressure is a parameter of paramount importance in the design of offshore pipelines [1–5] and is also affected by the bending curvature in the sagbend region of the pipeline. Upon reaching a maximum pressure, the pipe becomes unstable, and its cross section obtains an oval-shape and eventually a dog-bone shape, due to the accumulation of plastic deformation at the locations of maximum circumferential curvature change, which act as plastic hinges, leading to inner pipe wall contact and cross-sectional flattening [6]. The flattened configuration is initially limited to a few pipe diameters, and it may propagate along the pipeline when the external pressure level exceeds the propagation pressure $P_p$, which is significantly lower than $P_c$ ($P_p < P_c$). Figure 1 shows the deformed configuration of a pipeline at the onset of localized collapse and during buckling propagation.

Welded pipes undergo substantial plastic deformation during their manufacturing due to cold forming process, which affect significantly the material properties compared to the initial raw material. Cold formed pipes are fabricated from steel plates or steel coils. The most popular methods to fabricate pipes of medium or large size are the UOE and JCO-E processes, which employ steel plates. The acronyms of those fabrication methods refer to the shape of the cold bent plate at each manufacturing step. Previous works on pipes fabricated by the JCO-E and UOE process [7–10] have demonstrated the effects of cold bending and expansion on the collapse capacity of the final product. During the expansion stage, the pipe material is deformed up to a high level of tensile strain, to improve the cross-sectional imperfections, reducing cross section out-of-roundness and alleviating residual stresses.

[1]Corresponding author.

Contributed by the Ocean, Offshore, and Arctic Engineering Division of ASME for publication in the Journal of Offshore Mechanics and Arctic Engineering. Manuscript received December 22, 2025; final manuscript received May 2, 2026; published online June 22, 2026. Assoc. Editor: Dimitrios G. Pavlou.

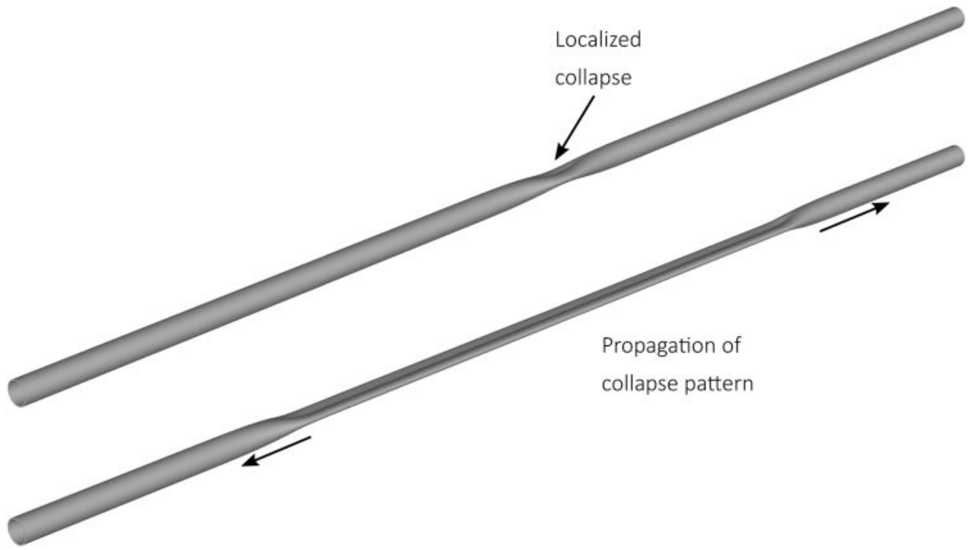


**Fig. 1 Numerical representation of localized collapse and its propagation in a steel pipe under quasi-static steady-state conditions**

However, the compressive strength, during reverse loading under external pressurization, is degraded due to the Bauschinger effect resulting in reduced pipe collapse capacity.

The present work investigates experimentally and numerically the collapse performance of high-frequency welded (HFW) pipes. Those pipes are manufactured by gradual bending of a steel coil into a circular shape through a series of rolls. Figure 2 shows the HFW manufacturing process, which is a continuous process, consisting of five mechanical steps [3]: (a) uncoiling, where the base material (coil) is unfolded; (b) leveling, where the steel sheet is flatted using a series of rollers; (c) roll-forming, where the sheet is deformed through a series of rollers to obtain progressively a circular shape; (d) welding of the pipe edges takes place using the high-frequency induction method, which does not require welding consumables; (e) passing the circular geometry through a series of sizing rollers (sizing process) to reduce the geometric imperfections of the pipe after heat treatment and inspection of the welding area. Finally, the continuous pipe is cut into parts of appropriate length to obtain the final line pipes [3].

HFW pipes are increasingly favored in the pipeline industry for medium size pipes (up to 26-in. diameter), due to their continuous fabrication procedure, compared to the other cold-formed pipes (JCO-E and UOE), where a specific-length plate is deformed during different stages. Therefore, the HFW process results in high production speed and reduced manufacturing costs, avoiding the use of expensive forming presses and equipment for

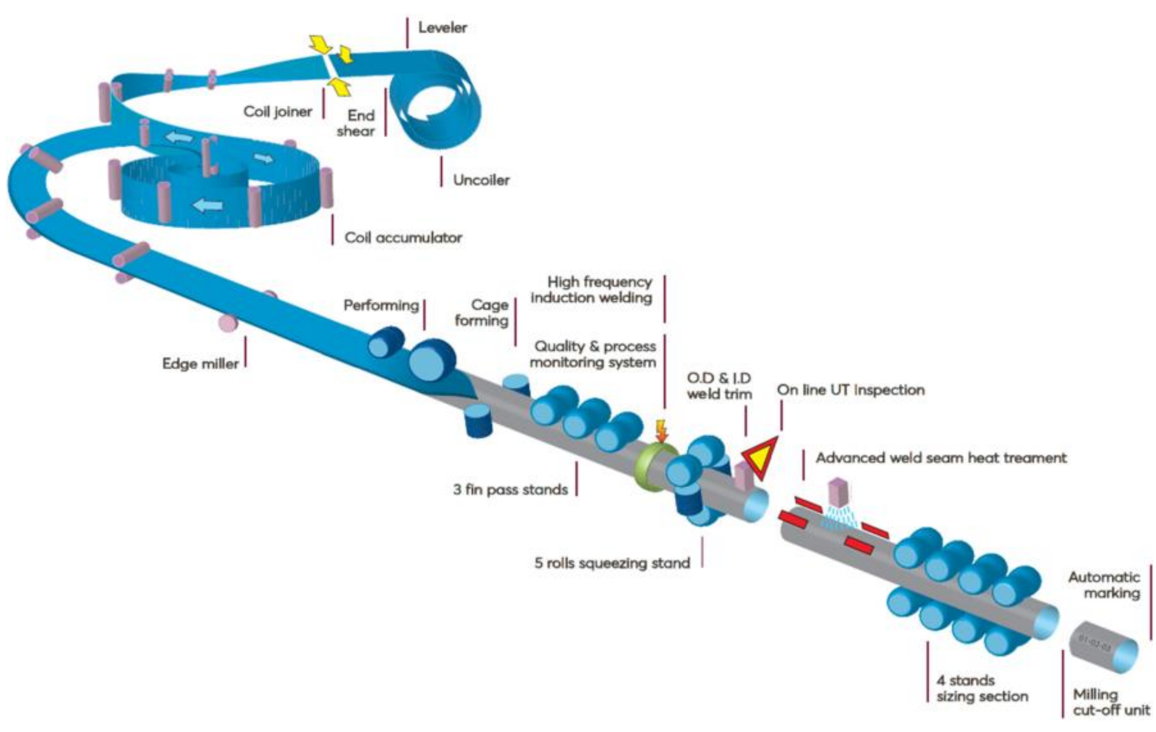


**Fig. 2 Schematic representation of the HFW pipe manufacturing process (courtesy of photo: Corinth Pipeworks S.A.)**

mechanical expansion. Additionally, high-frequency induction welding is faster and consumes less energy than submerged arc welding used in UOE/JCO-E processes. Previous works on HFW pipes focused primarily on the welding process. Asperheim et al. [11] developed a finite element model to simulate and optimize the high-frequency induction welding process. Moreover, Kang et al. [12] and Techmański et al. [13,14] investigated the effect of welding parameters on the quality assurance of the weld related to its shape and the HAZ. On the other hand, the effect of the HFW pipe fabrication process on pipe collapse capacity has not been investigated in depth.

So far, the use of HFW pipes in deep offshore applications has been limited. However, their cost-efficient fabrication makes those pipes very promising for deep-water pipeline projects. Toward that purpose, the structural strength and performance of HFW pipes under external pressure should be investigated, and this constitutes the primary motivation of the present research, which is supported by the pipe industry. Furthermore, the research addresses for the first time the issue of mild heat treatment effect on HFW pipe collapse, through a comprehensive methodology that includes full-scale and small-scale testing numerical modeling and analytical work.

Modeling of the HFW cold forming process has attracted some attention in the past. Wen and Pick [15] and Kiuchi et al. [16] developed finite element models to investigate the effect of roll-forming step (c) on pipe edge buckling. More recently, Lee et al. [17] developed numerical models to simulate the roll forming steps of the process and estimated the reduction of yield stress and the Bauschinger effect during repeated cyclic loading at a material point. Moreover, Han et al. [18,19] developed a numerical methodology for simulating the steps of roll-forming (c) and sizing (e) of the HFW manufacturing process. Their results show that the sizing step is crucial for the properties of the line pipe, affecting the compressive hoop strength and the collapse pressure, due to the Bauschinger effect. More recently, Tran et al. [20,21] using numerical simulation investigated the effect of the sizing process on the collapse capacity of ERW pipes under uniform external pressure, and combined external pressure and bending loading conditions. The numerical results demonstrated that the collapse pressure is affected by the compressive hoop strength degradation during the cold-forming process, which also depends on the sizing ratio. This effect is also documented in design standard DNV-ST-F101 (2021) [22], considering a fabrication factor equal to 0.93 for HFW pipes which reduces the external pressure capacity. However, the degradation of material properties of cold-formed pipes may be mitigated by applying a mild heat treatment process of short duration on the fabricated line pipe, as reported in previous works [4,5,23–29]. These works have indicated that mild heat treatment facilitates the recovery of compressive hoop strength of the line pipe resulting in increased collapse capacity of the "heat treated" pipe, with respect to "as fabricated" pipe. In DNV-ST-F101, the recovery of the strength due to heat treatment or external cold sizing (compression) allows the fabrication factor to be increased.

The present research is motivated by the need of pipeline industry to determine the collapse strength of HFW for the purpose of using those pipes in deep offshore applications. The work combines experimental work with numerical simulations to investigate the collapse performance of HFW pipes and to verify their suitability for use in deep-water pipeline applications. Special emphasis is given on the recovery of compressive hoop strength and the relevant increase of collapse pressure after a mild heat treatment process, which occurs during the external coating process. Two HFW pipes from the same heat are full-scale tested to collapse and to subsequent buckle propagation in a special-purpose pressure chamber. One pipe is coated ("heat treated"), using a mild heat treatment method, while the other pipe remained uncoated ("as fabricated" or "bare"). Before full-scale testing, coupon specimens are extracted from each pipe and subjected to uniaxial compression, in order to obtain the compressive stress–strain curve of the material and identify the effect of coating on the material strength recovery compared to the material of the bare pipe. During full-scale testing, unique strain measurements are obtained, using a strain-gauge system that operates within a highly pressurized water environment. The full-scale collapse tests are numerically simulated using a simple and efficient volume-control methodology, based on a new special-purpose scheme, which overcomes numerical convergence issues, associated with contact of deformable surfaces. The experimental and numerical values of collapse and propagation pressure are also compared with the predictions of DNV-ST-F101 (2021) design standard. Furthermore, the influence of different compressive hoop stress–strain curves on the collapse capacity, related to different levels of material strength recovery, as well as the relevant effect of the diameter-to-thickness ratio are investigated.

## 2 Experimental Procedures

The experimental work of this study involves primarily full-scale testing for collapse and buckle propagation of two pipe specimens, from the same heat, produced by Corinth Pipeworks S.A. (CPW). One pipe is subjected to a mild heat treatment process at 230 °C for approximately 1 minute which is typical for those pipes during their coating process. This is referred to as "coated," while the other specimen remained "as fabricated," also referred to as "bare." To support the full-scale tests and the numerical simulations, material characterization of two HFW pipes is conducted. The mechanical properties of both materials are obtained through a series of uniaxial compression tests on coupon specimens oriented circumferentially extracted from different locations around the circumference of pipe samples.

### 2.1 Material Testing and Mechanical Behavior.

To identify the properties of the bare ("as fabricated") and coated ("heat treated") material, rings of 400 mm in length were cut out from both line pipes produced by CPW. In each ring, a cross section was selected in which the positions that specimens would be obtained were marked. These positions, namely 90 deg, 180 deg, and 270 deg were selected, with 0 deg corresponding to the position of the weld, as shown schematically in Fig. 3. At these positions, strip full-thickness samples of the ring are extracted, and coupon specimens are machined from the inner and the outer part of every strip sample. The actual coupon specimen geometry adopted in this study is shown in Figs. 4(*b*) and 4(*c*). The coupon specimens are extracted from the circumferential direction of the pipe samples to account for the transverse material properties in

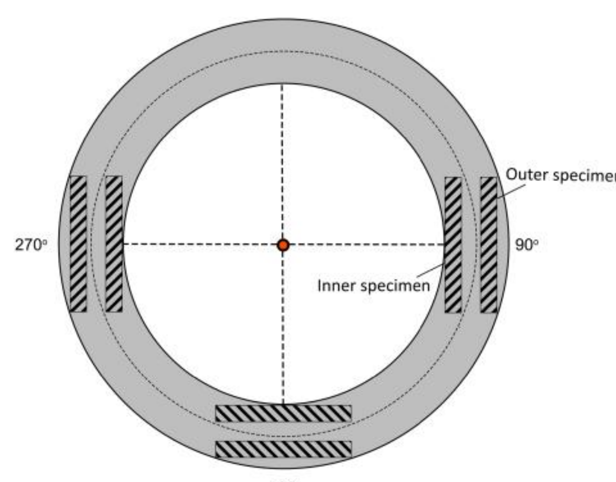


**Fig. 3 Locations of coupon specimens with circumferential orientation with respect to the center of pipe**

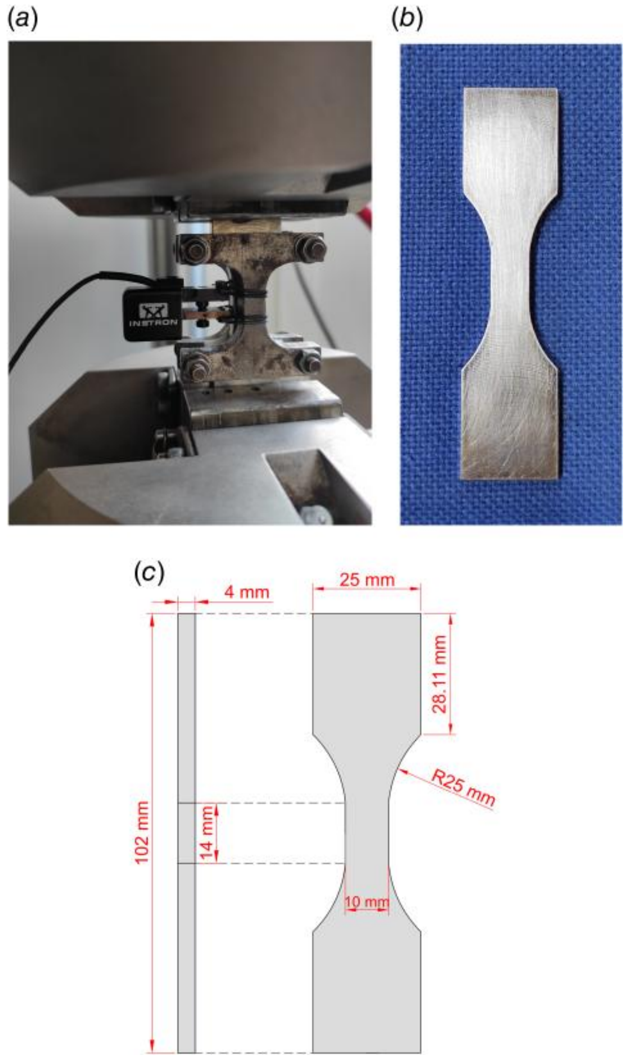


**Fig. 4 Experimental setup used in material tests (*a*) on coupons machined from the bare and coated HFW pipes according to SEP 1240 (2006) provisions (*b* and c); in the setup, the I-shaped antibuckling device is shown**

the form of the circumferential yield strength which influences the collapse pressure of pipes in deep-water applications [5,30]. The specimen geometry and the testing procedure is based on the provisions of SEP 1240 (2006) [31] guideline. The compression tests are performed using an antibuckling device to avoid buckling of the specimen and an INSTRON dynamic extensometer with gauge length of 10 mm, as shown in Fig. 4(*a*). All material tests are performed under a constant displacement rate of 0.25 mm/min, which is applied to the lower grip of the testing machine. The mechanical tests are conducted in the universal 100-kN INSTRON machine of the Laboratory of Mechanics and Strength of Materials (MSM), of the University of Thessaly.

The material properties at the selected locations, where the specimens correspond, were obtained in the form of stress–strain curves. Every specimen is tested in compression until 1% of total strain. Figure 5 shows the compressive stress–strain curves at 90-deg location at the inner and the outer parts of the pipe wall for the bare pipe material. Comparing the compressive yield stress at 0.5% of total strain between the inner and outer stress–strain curves, it is shown that the compressive yield strength is significantly lower at the outer part of the pipe, where tensile plastic deformation occurs during bending of the uncoiled steel plate on the rollers. Similar curves obtained for the other locations around the circumference. The yield stress ($\sigma_{y,B}$) at the inner and the outer part at 90-deg location is 573.3 MPa and 512.6 MPa, respectively. The results show that the yield strength at the outer part is approximately 10% lower than the yield strength at the inner part in each location around the circumference. The reduced yield strength at the outer part of the wall thickness, is in agreement with previous observations in JCO-E pipes [5,30] and it is a direct consequence of the cold forming process.

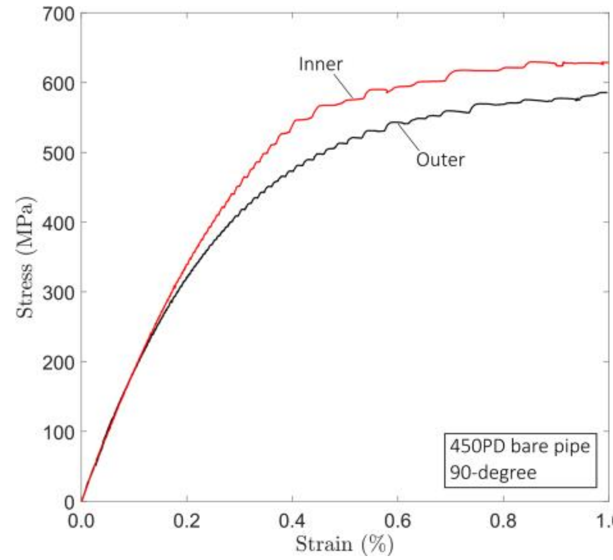


**Fig. 5 Compressive stress–strain curves from coupons extracted from the inner and outer parts of the bare ("as fabricated") pipe in the circumferential direction at 90-deg location**

The effect of heat treatment on the material properties is shown in terms of the increase of the yield strength at the outer part of the "heat treated" pipe material (coated pipe) compared to the yield strength at the outer part of the "as fabricated" pipe material (bare pipe). Figure 6 shows the compressive stress–strain curves at 90-deg position of the outer part before and after heat treatment. The yield stress at 0.5% of total strain is 512.6 MPa and 574.7 MPa for the bare pipe material and the coated pipe material, respectively, showing that the compressive strength of the coated material

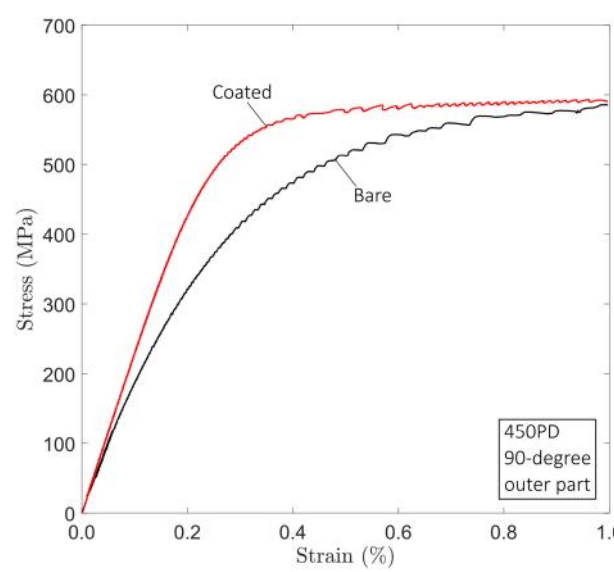


**Fig. 6 Compressive stress–strain curves obtained at 90-deg outer position from circumferential specimens machined from the coated and bare pipes**

Table 1 Yield strength at 0.5% of total strain for the bare and coated material at different positions of the outer and inner surface

| Position | | Bare | Coated | Difference (%) |
|---|---|---|---|---|
| 90 deg | Inner | 573.3 | 642.8 | 12.1 |
| | Outer | 512.6 | 574.7 | 12.1 |
| 180 deg | Inner | 530.7 | 661.3 | 24.6 |
| | Outer | 593.4 | 607.4 | 2.4 |
| 270 deg | Inner | 647.5 | 659.5 | 1.9 |
| | Outer | 540.3 | 573.4 | 6.1 |

is significantly affected. The yield stress of the coated pipe material at the 90-deg outer position increases by 12.1%, while similar behavior is observed at the other locations around the circumference. The yield stress at 0.5% of total strain for each position around the circumference for the inner and outer surface is summarized in Table 1. The test results show that the compressive strength of the coated material is increased with respect to the bare pipe material, while the highest increase of 12.1% in yield stress is observed for the 90-deg position in the outer surface. Additionally, the proportional limit stress at 90-deg position of the outer part, before and after heat treatment, is 100 MPa and 446.3 MPa, respectively.

**2.2 Full-Scale Collapse Testing.** Collapse testing of the bare and coated pipe specimens was conducted in C-FER facilities in Edmonton at their deep-water experimental chamber (DEC). The DEC has a pressure capacity of 62 MPa, and a normal maximum operating pressure of 55 MPa. The inside diameter is 1.2 m and its total inside length is 10.3 m. The two end-capped pipe specimens of length equal to $17D_o$ (corresponding to a length of 7 m) were water-filled without pressure and inserted into the chamber. The application of external hydrostatic pressure to each specimen was applied using a volume-control scheme, controlling the rate of external pressure increase through a variable frequency drive (VFD) pump motor. Testing was continued beyond buckle formation at collapse, allowing for the buckle to propagate along the pipe specimen, reaching its ends. The collapse and propagation pressure of every pipe specimen was measured. The volume change enclosed by the specimen was measured by monitoring the amount of water expelled from the collapsing pipe, using a port in one end cap with tubing extending outside of the pressure vessel, which remains open to atmosphere. The experimental instruments used in testing, consist of pressure transducers and water volume measurements, while data acquisition analysis was made, using LABVIEW software package. Figure 7 presents the post-test configuration of the collapsed and flattened bare pipe specimen (Figs. 7(*a*) and 7(*d*)) and the coated pipe specimen (Figs. 7(*b*) and 7(*e*)). Figure 7 also depicts the collapse configurations of the numerical simulations, described in Sec. 3, for comparison.


**Fig. 7 Deformed configuration of the as fabricated (bare) pipe specimen (*a* and *d*) and the coated pipe specimen (*b* and *e*) after the full-scale collapse test and the corresponding configuration obtained using the finite element model of Sec. 3 (*c* and *f*)**

The geometric characteristics of both specimens were determined prior to testing. Both specimens were grid-marked. The bare pipe was marked with a grid composed of 153 points, consisting of 17 circumferential locations (Fig. 8(*a*)) and 9 longitudinal stations (Fig. 8(*b*)), while 4 longitudinal stations (Fig. 8(*c*)) and 17 circumferential locations were marked on the coated pipe composing a grid of 68 points due to the 3-layer polypropylene (3LPP) of the outer surface. The methodology followed for the pipe marking process is similar to the one described Gavriilidis et al. [5]. For both pipes, measurements of outer diameter ($D_o$) and wall thickness (WT) are obtained in every longitudinal station (Figs. 8(*b*) and 8(*c*)) using a Dakota Ultrasonics hand-held thickness scope (MVX model A). The geometric measurements for both pipes are summarized in Table 2, including the minimum, maximum, average and standard deviation (SD) values of $D_o$ and WT. In this table, additional measurements of ovality parameter $O_o$, length ($L$), and circumference ($C$) are also presented. The ovality parameter ($O_o$) is calculated considering the outer diameter measurements and the following formula proposed by the DNV-ST-F101 (2021) design standard:

$$O_o = \frac{D_{o,\max} - D_{o,\min}}{D_o} \qquad (1)$$

where $D_o$ is the nominal outer diameter, $D_{o,\max}$ is the maximum measured outer diameter, and $D_{o,\min}$ is the minimum measured outer diameter at the same cross section.

Furthermore, for the first time in such high-pressure experiments, underwater strain gauges (model KFGS-2-350-C1-11) are placed on the outer surface of the bare pipe specimen to record

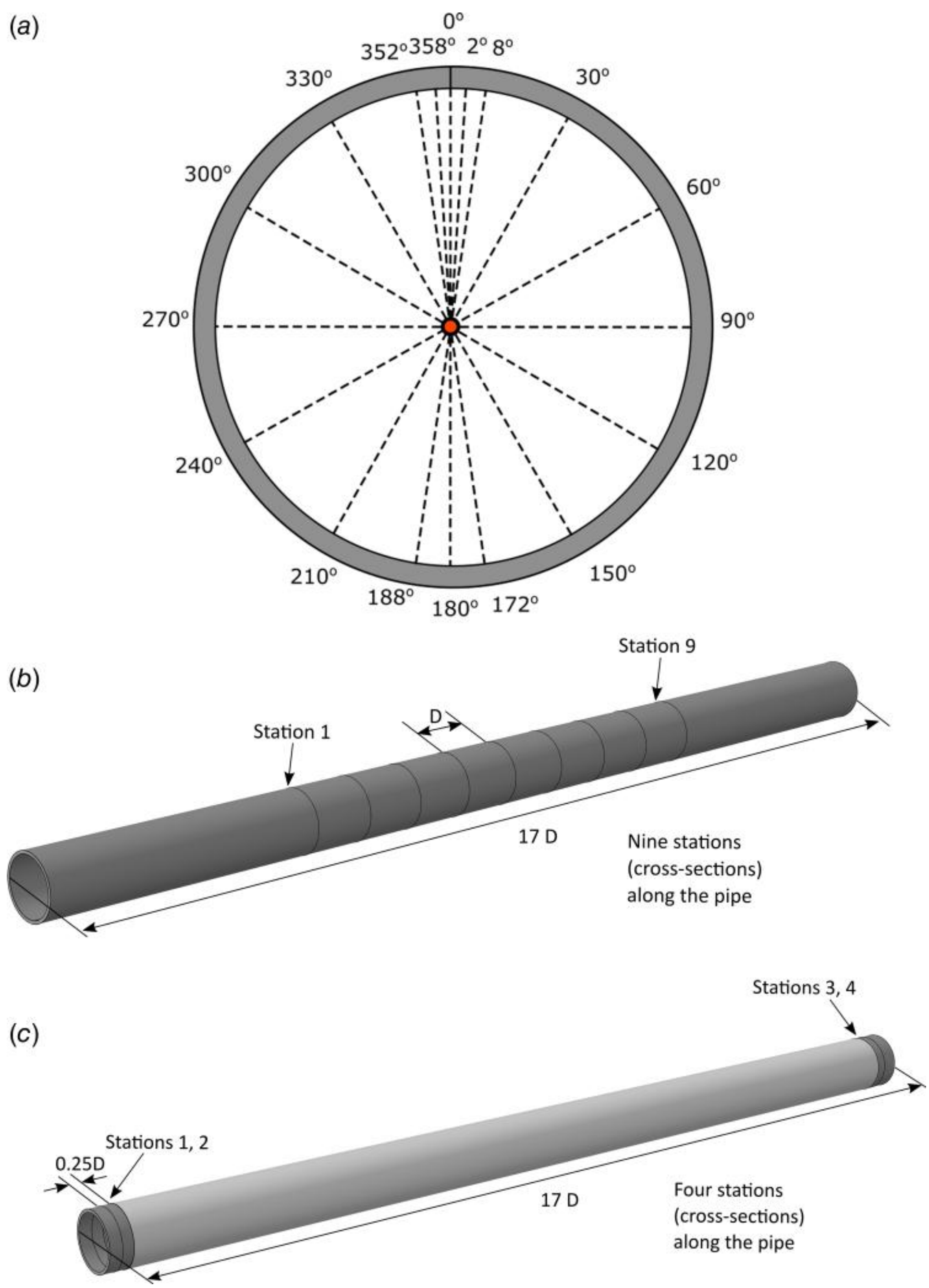


**Fig. 8 Grid of points used to measure diameter, ovality and thickness (*a*) around the circumference of both specimens (0 deg: high-frequency welding location), (*b*) in the longitudinal direction of the bare specimen, and (c) in the longitudinal direction of the coated specimen**

Table 2 Prior to testing measurements of WT, cross-sectional ovality ($O_o$), outer diameter ($D_o$), length ($L$), and circumference ($C$) of the bare and coated pipe specimens

| Measurements | Bare specimen | Coated specimen |
|---|---|---|
| WT (mm) | | |
| Maximum WT | 20.2 | 20.1 |
| Minimum WT | 19.3 | 19.0 |
| Average WT | 19.6 | 19.4 |
| SD WT | 0.2 | 0.2 |
| $D_o$ (mm) | | |
| Maximum $D_o$ | 409.1 | 408.1 |
| Minimum $D_o$ | 407.0 | 406.9 |
| Average $D_o$ | 407.9 | 407.5 |
| SD $D_o$ | 0.4 | 0.3 |
| $O_o$ (%) | | |
| Maximum $O_o$ | 0.4 | 0.3 |
| Minimum $O_o$ | 0.2 | 0.2 |
| Average $O_o$ | 0.3 | 0.3 |
| $L$ and $C$ (mm) | | |
| Average L | 6998 | 6985 |
| Average C | 1283 | 1282 |

the hoop (circumferential) strains during the full-scale collapse test. The expected location of buckling along the pipe specimen and its orientation, which are necessary to determine the optimum position of the strain gauges, are obtained from preliminary finite element analyses, using the geometric measurement of the bare pipe specimen presented in Table 2. Based on those preliminary numerical results the strain gauges are placed at the predicted locations of plastic hinges "PH1" (30 deg), "PH2" (120 deg), "PH3" (210 deg), and "PH4" (300 deg), at station 5 of the bare pipe, as shown in Fig. 9. Furthermore, it is expected that at the outer surface locations, "PH1" and "PH3" deform under compression, while "PH2" and "PH4" deform under tension, considering the dog-bone shape of the flattened cross section. The experimental results in terms of collapse and propagation pressure, also in terms of measured strains, are compared with numerical predictions in Sec. 4.1.

## 3 Finite Element Model

The actual pipe has been modeled simulating the pipe response under external pressure, similar to the models employed in

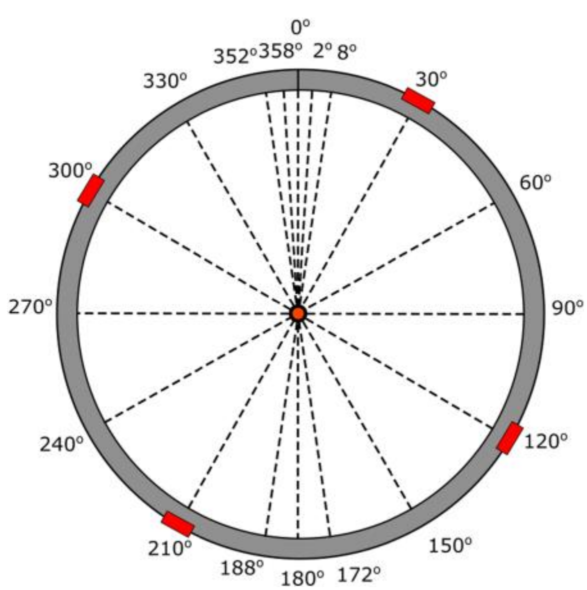


Fig. 9 Underwater strain gauges on the bare pipe placed at "PH1," "PH2," "PH3," and "PH4" of axial station 5


Fig. 10 Three-dimensional finite element model of pipe specimens

previous works of the authors [4,5]. The three-dimensional finite element model is developed in ABAQUS/STANDARD [32]. The model is capable of capturing the actual orientation of the collapsed configuration of the pipe specimens, shown in Fig. 7, and predicting the collapse and propagation pressure of HFW pipes in an accurate manner. The numerical results of collapse and propagation pressure are presented and discussed in Sec. 4.2.

Figure 10 shows the finite element model of the bare pipe specimen. The actual measurements of the outer diameter and wall thickness are obtained for the bare pipe at the stations presented in Fig. 8(*b*). These measurements are used to create the three-dimensional finite element model of the bare pipe, shown in Fig. 10. The end cross sections of the model at $z = 0$ and $z = L$ have the nominal dimensions of the pipe; the outer diameter of the pipe is 406.4 mm and the wall thickness is 19.1 mm. The model is seventeen outer diameters long ($L = 17D_o$), representing the length of the full-scale actual pipe specimen, described in Sec. 2.2. The end sections of the pipe model at $z = 0$ and $z = L$ are fixed representing the boundary conditions imposed during the actual full-scale test. In the case of the coated pipe, fewer measurements were available, due to the presence of the 3LPP external coating layer, as shown in Fig. 8(*c*). Therefore, the measurements of the bare pipe are also employed to reproduce the geometry of the coated finite element model, as shown in Fig. 10.

A new feature of the numerical model refers to the methodology used for advancing the solution beyond initial collapse and obtain the consecutive stages of progressive collapse and its steady-state propagation. This process is closely related to the experimental procedure, it is inspired by the volume-like parameter introduced by Tassoulas et al. [33], and overcomes the convergence issues that occur when the more traditional arc-length (Riks) method is used. Alternative volume-control schemes have also been reported by Kyriakides and Lee [2] using fluid elements around the pipe specimen and Fu et al. [34] who employed a surface-based fluid-filled cavity and used the "fluid exchange" feature in ABAQUS. Herein, the volume-control scheme is implemented in a simple and efficient manner considering a fluid cavity filled with water that corresponds to the enclosed volume of the capped pipe as shown in Fig. 10. Translating outwards the caps at both ends of the numerical model in the axial direction ($z$ direction), and using a static analysis step, increases the volume in the cavity leading in negative internal pressure, which is equivalent to external pressurization, simulating the nonlinear phenomenon of collapse and buckling propagation in a very simple and cost efficient manner. Considering the current numerical methodology, the time required for the numerical simulation of collapse and propagation of the HFW pipes under investigation is 8–10 times lower in comparison with the classical Riks' method.

The geometry of the pipe model is discretized with 24,000 20-node reduced-integration quadratic hexahedral elements, denoted as C3D20R in ABAQUS. The mesh of the pipe finite element model consists of 80 and 150 elements in the circumferential and longitudinal direction, respectively, adopting the mesh density reported by Gavriilidis et al. [5] after conducting a sensitivity analysis. The caps at both ends of the model are discretized with 8-node reduced-integration linear hexahedral elements, denoted as C3D8R in ABAQUS, using 80 elements and 1 element in the circumferential and longitudinal direction, respectively. Frictionless contact, accounting for self-contact of the pipe inner surface, is assumed to obtain the expected dog-bone collapsed shape of Fig. 7. Furthermore, the "Direct" feature of ABAQUS for hard pressure-overclosure behavior is employed, also used by the authors in a previous work with very good results [5].

The circumferential compressive stress–strain material data of the outer part are assigned as material properties of the bare and coated pipe models (Fig. 10). The material properties in the circumferential direction of the outer surface of the pipe account for the most severe material degradation, due to the cold-bending fabrication process [4,5,30,35]. An average stress–strain curve is used for the bare and coated pipe material, which is obtained by the stress–strain curves at 90-deg, 180-deg, and 270-deg locations, following a procedure similar to the one presented in previous works of the authors [4,5]. The yield stress of the averaged curve measured at 0.5% of total strain is 548.0 MPa and 595.4 MPa for the bare and coated pipe material, respectively, while the corresponding proportional limit stress values are 126.5 MPa and 415.5 MPa for the bare and coated pipe material, respectively. The Young's modulus ($E$) and Poisson's ratio ($\nu$) are equal to 210 GPa and 0.3, respectively. Figure 11 presents the averaged stress–strain material curves of the bare pipe and the coated pipe, used in the finite element models. The yielding and hardening behavior of the pipe material is described by a $J_2$ (von Mises) flow plasticity model with isotropic hardening properly calibrated with the stress–strain curve under consideration.

## 4 Numerical Results

The full-scale collapse tests of the bare and the coated pipe are simulated using the numerical methodology presented in Sec. 3. The equilibrium diagram is obtained for each pipe model showing the variation of external pressure in terms of the change of volume enclosed by the pipe, and it is compared with the corresponding experimental curve. In particular, the numerical predictions of the collapse pressure and the propagation pressure are compared with the corresponding experimental values. Different stress–strain material curves, corresponding to different levels of heat treatment, are considered to investigate the effect of compressive strength recovery on the collapse capacity of HFW pipes.

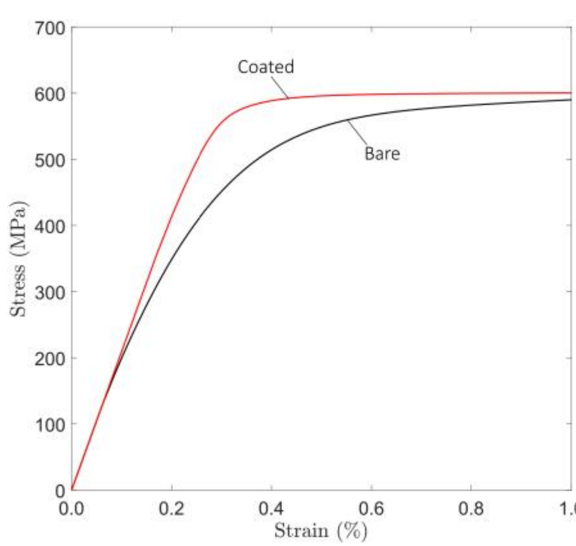


**Fig. 11 Compressive stress–strain curves of the bare and coated pipe material obtained by averaging the stress–strain curves around the circumference for each material**

Additionally, the effect of mild heat treatment on a pipe with different diameter-to-thickness ratio is examined. The numerical predictions and the experimental values of collapse and propagation pressure are also compared with the corresponding estimates from the DNV-ST-F101 (2021) design standard.

### 4.1 Collapse and Propagation.

The variation of external pressure with internal volume change, obtained from the numerical simulation of the bare pipe experiment, is shown in Fig. 12(*a*). The volume change is calculated in a postprocessing stage, using the inner surface node coordinates during the numerical analysis. The external pressure $P$ is normalized by the yield pressure of the pipe ($P_y$):

$$P_y = 2\sigma_{y,n}\frac{t}{D_o - t} \quad (2)$$

where $\sigma_{y,n}$, $D_o$, and $t$ are the specified minimum yield stress of 450 PD steel material (450 MPa), the nominal outer diameter value of the pipe (16 in.), and the average value of pipe wall thickness measured before testing, as shown in Table 2. The volume change, $\Delta V$, is normalized by the initial volume enclosed by the pipe ($V_o$). Figure 12(*a*) also shows the experimental equilibrium path obtained from the full-scale test of the bare pipe. The numerical results are in good agreement with the corresponding experimental curve in the prebuckling and the postbuckling regime of the equilibrium path. The experimental curve demonstrates an abrupt drop of pressure recorded between stages "1" and "3." This effect is due to sudden depressurization of the chamber immediately after collapse, and thus additional water pumping is needed to recover the external pressure level. Therefore, the pump is turned off, and the test is paused while the pressure is allowed to equalize between the pipe external and internal pressures. Once the pressures are equalized, the pump is turned on (rate VFD controlled). This phenomenon is also reported in previous works involving similar full-scale tests [5,36].

Figure 13 depicts the consecutive deformed configurations of the bare pipe model, during collapse and quasi-static steady-state buckling propagation. These pipe configurations correspond to the numbers on the equilibrium path, shown in Fig. 12(*a*). In Fig. 13, the cross-sectional configuration is rotated with respect to the $x$–$y$-axes. Initially, the external pressure increases until a maximum (ultimate) pressure is reached at stage "1," also referred to as "collapse pressure." Beyond collapse, the buckle localizes further and in that area postbuckling deformation is governed by a "four-plastic hinge" collapse mechanism, resulting in a significant reduction of external pressure, as shown at stage "2." The localized collapsed pattern, shown at stage "2," occurs at station 1 of the bare pipe model (Fig. 8(*b*)), where the maximum cross-sectional ovality is measured (0.4%), as shown in Table 2. Subsequently, the pressure decreases reaching a minimum pressure value at stage "3," where resistance of the collapsed cross section to further ovalization develops. This is referred to as "stiffening" and it is due to contact of two sides of the inner wall of the pipe, which also results in slight pressure increase. Beyond the "stiffening" state in the most deformed cross section of the pipe, instead of further cross-sectional flattening and pressure increase, the pipe finds it easier to deform the adjacent cross sections, on either side of the buckle until these cross sections reach a similar "stiffening" state. Repeatedly, a "steady-state" is reached, where each cross section enforces its adjacent one to deform, resulting in progressive collapse of the pipe and in propagation of the phenomenon at both directions along the pipe, as shown at stages "4" and "5" in Fig. 13, under constant pressure. This pressure value corresponds to the propagation pressure $P_p$. Propagation continues until the buckle reaches the ends of the model, as shown at stage "6," where fixed boundary conditions exist, and the external pressure increases as shown in the pressure-volume equilibrium path.

Figure 14(*a*) shows the cross-sectional configurations at station 1 of the bare pipe model in the postbuckling range at stages "1"–"3"

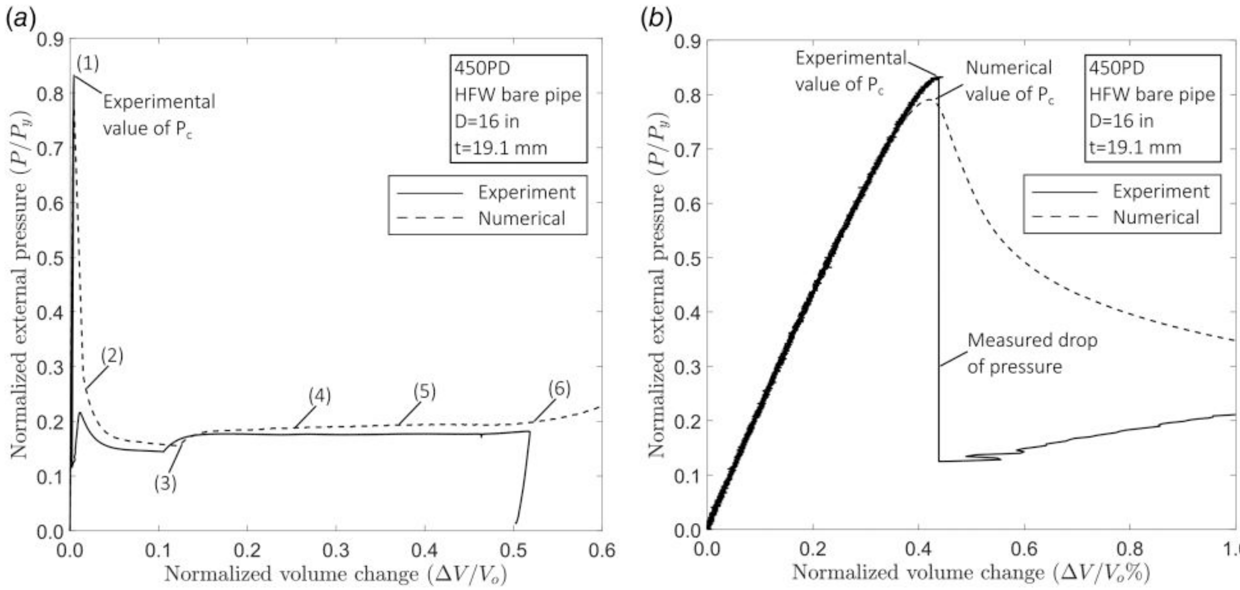


**Fig. 12 Equilibrium path showing the external pressure variation of the bare pipe with respect to (*a*) the total volume change; comparison between finite element simulation and full-scale experiment; (*b*) detail of (*a*) showing measurements and simulation during collapse**

of Fig. 12(*a*), while Fig. 14(*b*) presents the corresponding deformed configuration of the bare pipe during buckling propagation. The four equally-spaced plastic hinges "PH" formed around the circumference upon collapse, which drive the postbuckling phenomenon, are marked with dot points in Fig. 14(*a*). Their position is rotated by 31.5 deg with respect to the weld location (0 deg), which is very close to the orientation observed in the full-scale experiments (24 deg). The location of the plastic hinges for both the numerical model and the bare pipe specimen are summarized in Table 3. A good agreement is obtained for the location of each plastic hinge between the numerical results and the experimental test, and the difference in each location is less than 3%. Furthermore, Fig. 15 shows the variation of hoop strain at each plastic hinge with internal volume change, verifying the expected deformation mode at each location. The results show that the experimental and the numerical strain values are in good agreement up to collapse, denoted as the "maximum pressure" in Fig. 15. However, some differences between the experimental and numerical results are observed beyond collapse, possibly attributed to the abrupt change of geometry in the postbuckling stage. This issue requires more investigation but is out of the scope of the present article.

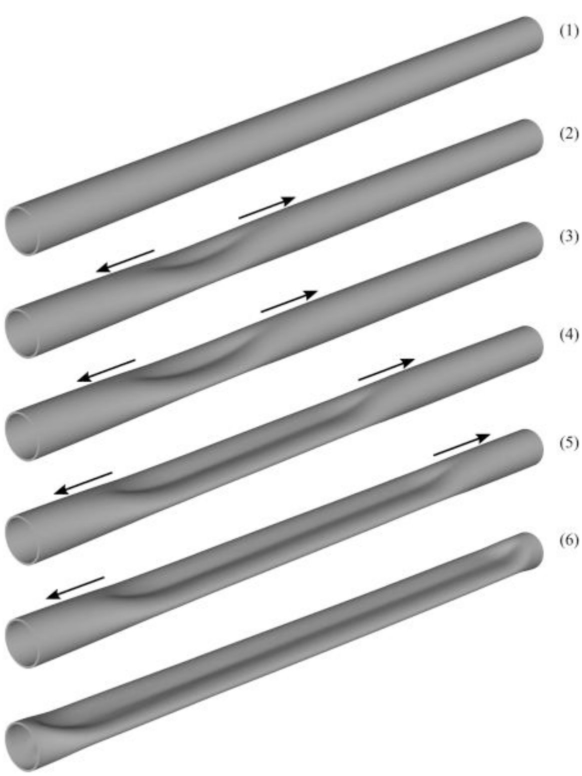


**Fig. 13 Deformed configurations of the bare pipe from the stage of maximum pressure to buckling propagation; the numbers next to each configurations are correlated with the corresponding numbers shown in the diagram of Fig. 12(*a*)**

The equilibrium path expressed in terms of external pressure variation with respect to the volume change is shown in Fig. 16 for the coated pipe. The external pressure is normalized by the yield pressure $P_y$ and the volume change is normalized by the initial volume $V_o$ enclosed by the pipe, such as the case of the bare pipe. The postbuckling configurations of the coated pipe are similar to those presented in Fig. 13 for the bare pipe. The postbuckling cross-sectional configuration of the coated pipe is also similar to the one shown in Fig. 14 for the bare pipe, in terms of flattening orientation and the location of plastic-hinges around the circumference. Additionally, it is very close to the experimental result (25 deg) shown in Table 3. The results indicate that both pipe specimens exhibit comparable geometric imperfections during the fabrication process. This implies consistency in the HFW manufacturing process and thus, the assumption of using the bare pipe initial geometry to simulate the full-scale test of the coated pipe is reliable. However, this argument arises from the full-scale tests performed in the present work. Additional experimental tests would be necessary to verify this observation.

**4.2 Comparison of Experimental Values and Numerical Predictions.** The numerical and the experimental results, in terms of both collapse pressure and propagation pressure, are in very good agreement for both pipe specimens, bare pipe and coated pipe. The numerical values of collapse pressure are 35.9 MPa and 43.9 MPa for the bare pipe and the coated pipe, respectively. These values are in good agreement with the corresponding experimental results, which are 38.0 MPa and 41.0 MPa for the

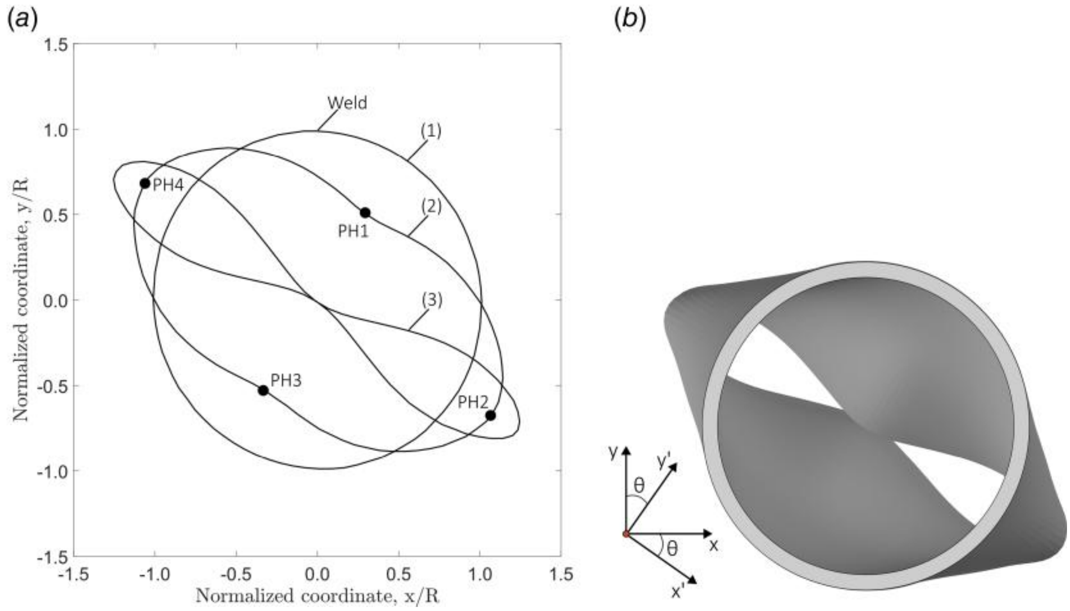


Fig. 14 (*a*) Deformed cross-sectional configurations at station 1 (inner surface) of the bare pipe model at different stages of postbuckling range; the numbers of the cross-sectional configurations are correlated with the corresponding numbers shown in Fig. 12(*a*), and the markings $PH_i$ ($i = 1, 2, 3, 4$) denote the location of the four plastic hinges. (*b*) Deformed configuration of the three-dimensional bare pipe model during buckling propagation. Orientation angle $\theta$ of the flattening shape is 31.5 deg.

**Table 3 Position of each plastic hinge (in deg) with respect to the weld location, obtained from the bare pipe numerical model and the corresponding experimental measurements from the bare and coated pipes**

| Plastic hinge location | Numerical simulation (deg) | Experimental value (bare) (deg) | Experimental value (coated) (deg) |
|---|---|---|---|
| PH1 | 31.5 | 24 | 25 |
| PH2 | 121.5 | 116 | 114 |
| PH3 | 211.5 | 204 | 205 |
| PH4 | 301.5 | 292 | 295 |

bare pipe and coated pipe, respectively. For the bare pipe, the difference between the numerical collapse pressure and the experimental value is 5%, while for the coated pipe the corresponding difference is 7%. The difference between the experimental and the numerical results for the case of the coated pipe model may be due to lack of the actual geometric properties of the coated pipe, due to external coating. Furthermore, this difference may also be attributed to inhomogeneous material properties of the pipe material or to different residual stress level of the bare pipe and the coated pipe, which is not considered in the present analysis. Therefore, the model is likely to underestimate the cross-sectional ovalization of the pipe in the coated area, by employing the bare pipe model in the analysis. The numerical values of the propagation

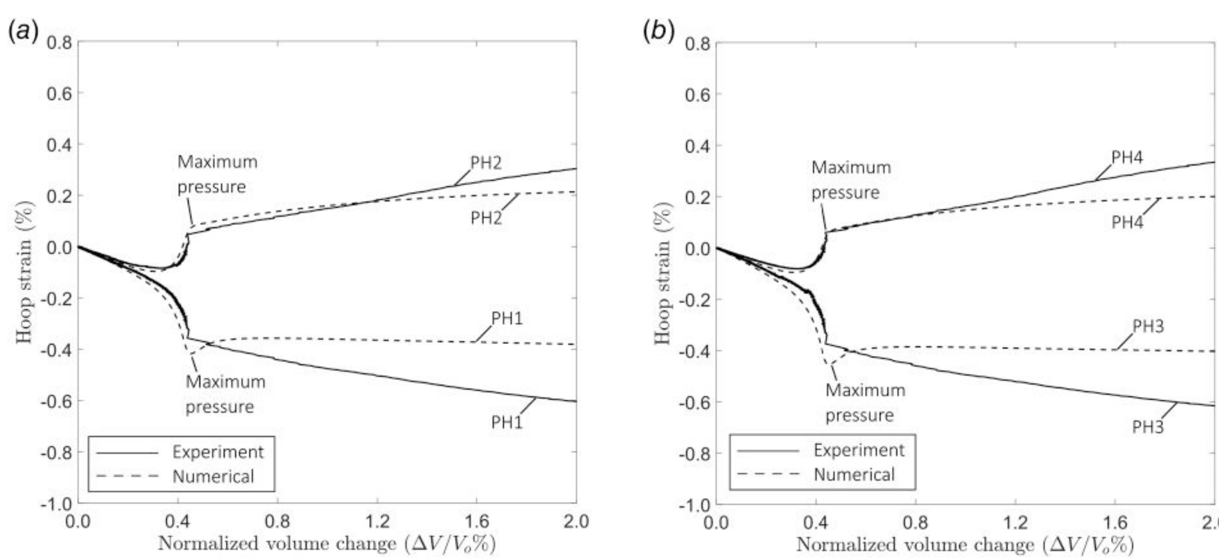


Fig. 15 Variation of experimental and numerical values of hoop strains with volume change corresponding to the plastic hinges (*a*) PH1 and PH2 and (*b*) PH3 and PH4, developed at station 5

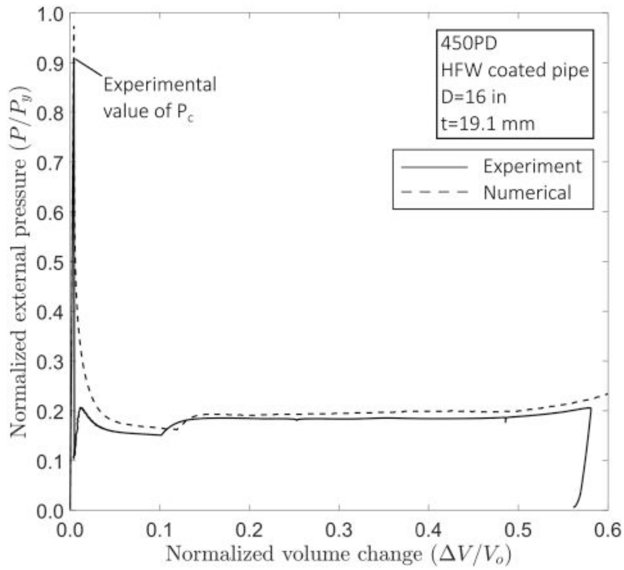


**Fig. 16 Equilibrium path showing the external pressure variation with respect to the volume change for the coated pipe; comparison between finite element simulation and full-scale experiment**

pressure are 8.3 MPa and 8.6 MPa for the bare pipe and the coated pipe, respectively, and they are in very good agreement with the corresponding experimental values, which are 8.0 MPa and 8.3 MPa for the bare pipe and the coated pipe, respectively. The difference between the numerical predictions and the experimental values for the propagation pressure is less than 4%. The results show that the propagation pressure is slightly increased by the mild heat treatment. This is attributed to the material strength recovery which is more pronounced between the range of 0.2%–0.6%, while beyond 0.6% both curves converge. Therefore, the mild heat treatment strongly affects the collapse capacity of the pipe which occurs in relatively small strain values than the propagation of the buckle which happens in higher strain values. The overall good agreement between experimental and numerical results indicates that the models developed in the present study are capable of simulating collapse and buckling propagation in an accurate manner. The numerical and experimental values of collapse and propagation pressure are summarized in Table 4.

**4.3 Comparison of Experimental Values and Numerical Predictions With Design Standard.** Collapse pressure and propagation pressure are also calculated with the DNV-ST-F101 (2021) design formula for the bare pipe and coated pipe. According to the standard, collapse pressure is obtained from the following expression:

$$(P_c - P_{el})\left(P_c^2 - P_{pl}^2\right) = P_c P_{el} P_{pl} O_o \frac{D_o}{t} \tag{3}$$

where $D_o$ and $t$ are the nominal values of the outer diameter (16 in.) and wall thickness ($t = 19.1$ mm) of the HFW pipe, respectively, and $O_o$ denotes the measured initial imperfection in the form of ovality defined by Eq. (1). The parameters $P_{el}$ and $P_{pl}$, in Eq. (3) denote the critical elastic buckling pressure and the plastic pressure, respectively, expressed as follows:

$$P_{el} = \frac{2E}{(1-\nu^2)}\left(\frac{t}{D_o}\right)^3 \tag{4}$$

$$P_{pl} = 2\sigma_{y,n}\alpha_{\text{fab}}\frac{t}{D_o} \tag{5}$$

where $E$, $\nu$, and $\sigma_{y,n}$ are the Young's modulus, the Poisson's ratio, and the specified minimum yield strength (450 MPa), respectively. Parameter $\alpha_{\text{fab}}$ is referred to as "fabrication factor" by the design standard and it is included in the expression of yield pressure to account for the degradation of compressive yield strength, due to the cold forming manufacturing. Additionally, the following expression is proposed by the DNV-ST-F101 standard for the calculation of the propagation pressure:

$$P_p = 35\sigma_{y,n}\alpha_{\text{fab}}\left(\frac{t}{D_o}\right)^{2.5} \tag{6}$$

According to the standard, $\alpha_{\text{fab}}$ parameter should be taken equal to 0.93 for HFW cold formed pipes, which is a value very close to the ratio of the yield stress at 0.5% strain of the bare pipe material (548.0 MPa) over the yield stress at 0.5% strain of the coated pipe material (595.4 MPa). The DNV standard allows for an increased value of $\alpha_{\text{fab}}$, when the pipe is heat treated. Herein, the fabrication factor $\alpha_{\text{fab}}$ is considered equal to 1 for the coated pipe. Considering the maximum value of ovality measured for each specimen, shown in Table 2, collapse pressure and propagation pressure are evaluated, using Eqs. (3) and (6). The results for each pipe are summarized in Table 4, showing also the corresponding experimental values and numerical predictions, presented in the previous section. The DNV-ST-F101 standard predictions are reasonable and capture well the collapse pressure increase, compared to the experimental values. However, the predictions are yet conservative and underestimate the collapse pressure and the propagation pressure by approximately 10%, compared to the corresponding experimental values. Nevertheless, considering the complexity of the collapse phenomenon, the DNV-ST-F101 equations can be used for safe prediction of the collapse and the propagation pressure, for design purposes.

**4.4 Effect of Mild Heat Treatment on the Collapse Pressure and Propagation Pressure.** The experimental and numerical results, presented in Sec. 4.2, indicate that the collapse pressure of the coated pipe increases compared with the bare pipe, because of the compressive strength recovery of the pipe material after the mild heat treatment. Al-Sharif and Preston [23] investigated the effect of different levels of heat treatment on the compressive stress–strain response of the pipe material, concluding that there is an upper limit of material strength recovery because of temperature increase. This scenario has also been examined in a previous work of the authors [5], where the stress–strain response of the steel plate, used to manufacture the JCO-E pipe, is adopted to represent the upper limit of the material strength recovery. The

**Table 4 Collapse pressure and propagation pressure (in MPa) of the 16-in.-diameter pipe specimens; experimental values, numerical results and DNV-ST-F101 predictions assuming $a_{\text{fab}}$ equal to 0.93 and 1 for the bare pipe and coated pipe, respectively**

| | Collapse pressure | | | Propagation pressure | | |
|---|---|---|---|---|---|---|
| Pipe | Experimental value | Numerical simulation | DNV-ST-F101 | Experimental value | Numerical simulation | DNV-ST-F101 |
| Bare | 38.0 | 35.9 | 34.0 | 8.0 | 8.3 | 7.0 |
| Coated | 41.0 | 43.9 | 36.9 | 8.3 | 8.6 | 7.5 |

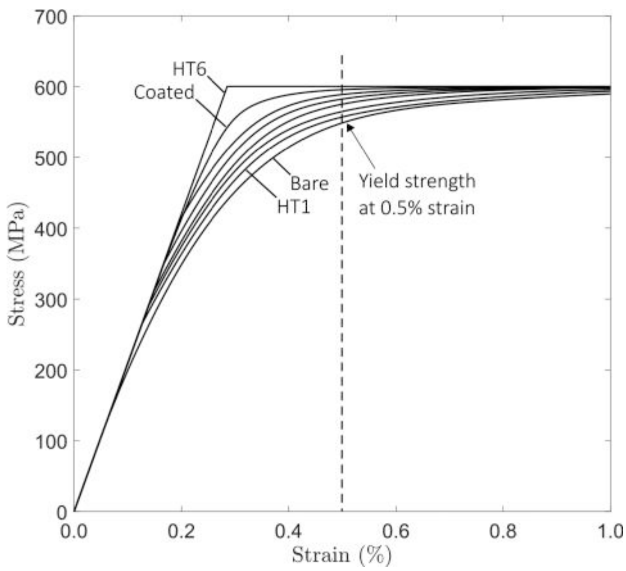


**Fig. 17 Compressive stress–strain responses considering different heat treatment levels, up to bilinear material curve (HT6)**

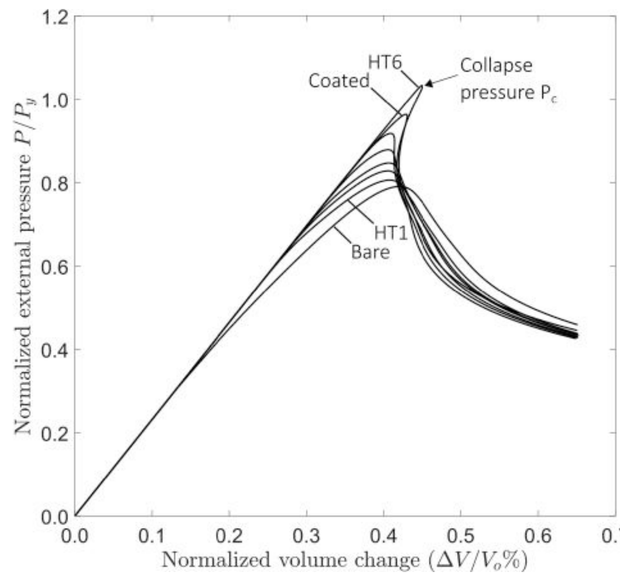


**Fig. 18 Variation of external pressure with volume change enclosed by the pipe, for the different material curves of Fig. 17**

**Table 5 Proportional limit stress and yield stress (in MPa) at 0.5% of total strain for different coating conditions**

| Level | Proportional limit stress | Yield stress |
|---|---|---|
| Bare | 126.5 | 548.0 |
| HT1 | 265.0 | 554.1 |
| HT2 | 290.0 | 562.9 |
| HT3 | 310.0 | 574.4 |
| HT4 | 350.0 | 582.3 |
| HT5 | 410.0 | 587.6 |
| Coated | 415.5 | 595.4 |
| HT6 | 600.3 | 600.3 |

present section investigates the effect of different material stress–strain curves on the collapse capacity of HFW pipes with gradually increasing yield stress from the bare pipe material curve to the plate material, represented by a bilinear curve. These curves may stem from different heat treatment conditions, resulting in different material strength recovery levels.

The stress–strain curve of the plate (HT6), shown in Fig. 17, is of a bilinear shape, and may be considered as the upper limit of material strength recovery, which theoretically corresponds to fully annealed material. Five additional stress–strain curves are considered (HT1, HT2, HT3, HT4, and HT5) with gradually increasing proportional limit stress and yield stress at 0.5% engineering strain from the bare pipe material to the coated pipe material, as shown in Fig. 17. The proportional limit increases by a substantial amount from the bare pipe material to the plate material. Furthermore, the yield stress at 0.5% total strain is 548.0 MPa and 600.3 MPa for the bare pipe material and the plate (HT6) material, respectively, while this corresponds to 10% increase, compared to the bare pipe material yield stress. The influence of heat treatment could also be expressed in terms of the plastic work dissipated during material compression, where the increase of the plastic work of each curve compared with the bare pipe material curve is

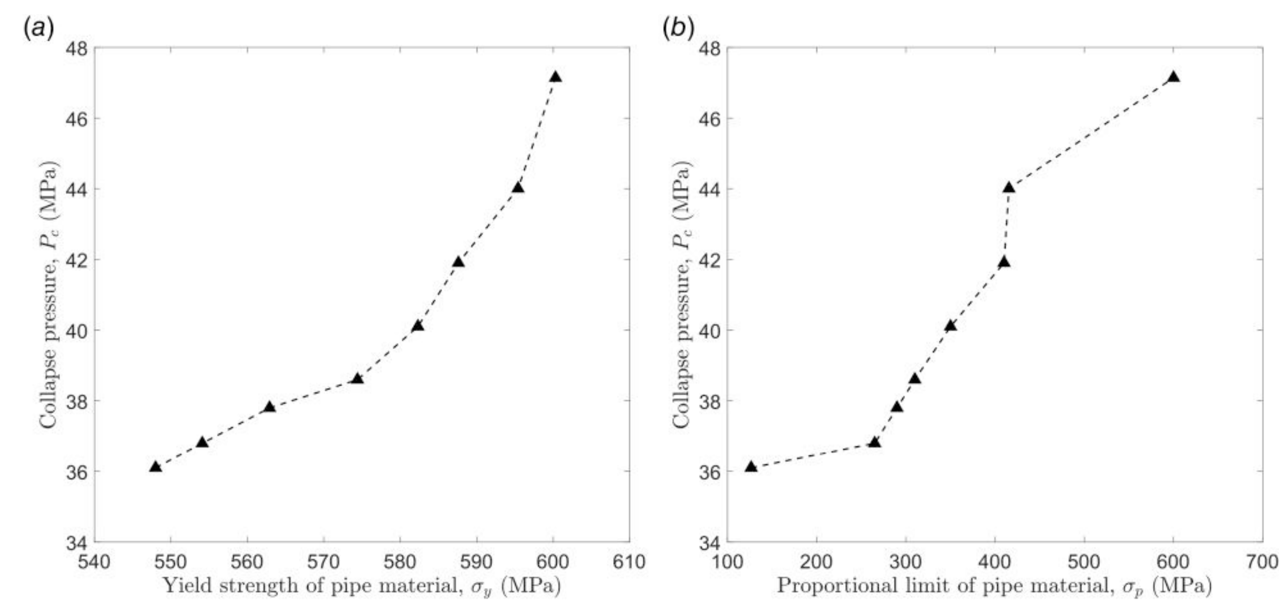


**Fig. 19 Collapse pressure with respect to the variation of (*a*) yield strength and (*b*) proportional limit of each curve presented in Fig. 17**

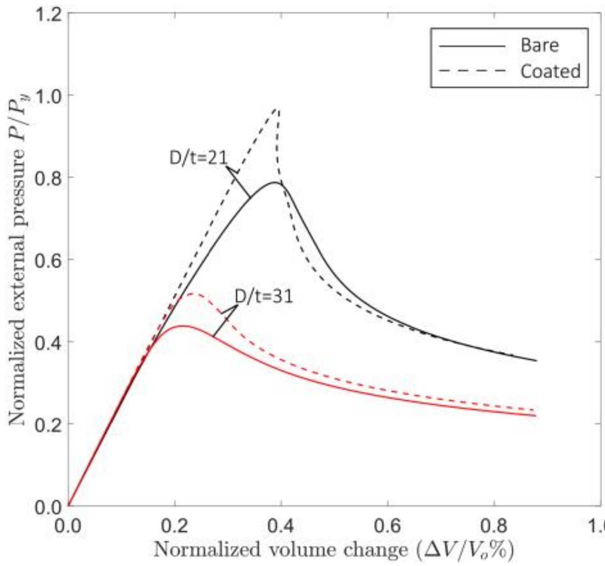


**Fig. 20 Variation of external pressure with volume change for the bare and coated pipes with $D/t$ equal to 21 and 31**

consistent with the increase of the yield stress. The values of the yield stress ($\sigma_y$) and the proportional limit ($\sigma_p$) for each curve are summarized in Table 5.

The material curves of Fig. 17 are employed in the numerical model described in Sec. 3, for the purpose of evaluating the influence of the material strength recovery on the collapse capacity. Figure 18 presents the variation of external pressure versus the volume change for each material curve. The collapse capacity for each material case ($P_c$) is increased with increasing the material strength recovery, indicating that the collapse resistance is significantly affected by mild heat treatment during line pipe coating. This is consistent with the results of a recent work of the authors [5], where the upper limit of material recovery has been adopted using a bilinear stress–strain curve from a plate material (before the pipe manufacturing process). In this case, the results show that the collapse pressure increases, indicating a strong dependence of collapse pressure with the proportional limit. This dependence is attributed to the fact that collapse occurs at relatively low levels of strain, lower than 0.5%. Considering HT1–HT5 material curves, the collapse pressure increases from 1.9% to 16.1% compared to the bare pipe, respectively, while the collapse pressure increases by 21.9% and 30.7% for the coated pipe and the plate material (HT6), respectively. Figure 19 also shows an increase of collapse pressure with increasing yield stress (Fig. 19(*a*)) and proportional limit stress (Fig. 19(*b*)) of the pipe material.

Furthermore, the effect of mild heat treatment on the collapse capacity of HFW pipes with different diameter-to-thickness ratio is investigated. A 16-in. pipe with wall thickness equal to 13.1 mm ($D/t = 31$) is simulated with a three-dimensional model, using the stress–strain curves shown in Fig. 11. Figure 20 shows the diagram of external pressure versus volume change for both $D/t$ cases (21 and 31). The results indicate that the beneficial effect of heat treatment on collapse pressure is less pronounced in thin-walled pipes. This is attributed to the smaller amount of plastic deformation associated with the collapse of thin-walled pipes, and also consistent with the DNV-ST-F101 predictions; for the bare pipe and the coated pipe those predictions are 14.1 MPa and 14.5 MPa, respectively, indicating a 3% increase for the pipe with $D/t = 31$, while the collapse pressure increase for the pipe with $D/t$=21 is 8%.

## 5 Conclusions

The collapse performance of HFW pipe was studied experimentally and numerically, motivated by the possible use of such pipes in deep offshore applications. Two 16-in.-diameter HFW pipes with 19.1 mm thickness, made of 450 PD steel grade from the same heat, have been subjected to full-scale collapse testing and, subsequently, their behavior was simulated numerically with nonlinear finite element models. The results demonstrated a very good performance of HFW pipes against collapse, which is the main parameter for the mechanical design of deep-offshore applications, indicating that those pipes are suitable for use in offshore pipeline projects. It was also shown that the application of mild heat treatment in the course of a typical coating process mitigates the detrimental effects of cold forming, leading to improved circumferential compressive yield stress, which is a key parameter for affecting the value of collapse pressure. The average increase in compressive yield stress due to the coating process is measured equal to 10%, which may have a substantial effect on the design of offshore pipes. Furthermore, the full-scale experimental results indicate that the collapse pressure is enhanced by 7.9% after coating, whereas the corresponding increase of the propagation pressure value is 3.8%.

The finite element models employ a simple and very efficient numerical technique introduced in the present article for tracing the unstable postbuckling path of the collapsing pipe, based on a volume-control scheme, which reduces the computational time by a substantial amount and minimizes convergence issues due to pipe inner surface contact. Considering averaged stress–strain curves from laboratory experiments on coupons extracted from the outer part of each pipe material (bare and coated), and using an initial geometry based on the actual geometric measurements, very good numerical predictions of the collapse and propagation pressure are obtained compared to the corresponding full-scale test results. The numerical results are also consistent with the full-scale experimental observations in terms of cross-sectional orientation of the pipe cross section and the locations of the four plastic hinges, which characterize the postbuckling shape. Additionally, excellent predictions are obtained with the strain measurements from the underwater strain gauges placed on the bare pipe for the first time during full-scale high-pressure testing, offering very useful insight into the progression of cross-sectional deformation in the postbuckling regime.

A short parametric study was also conducted, using the finite element models with compressive stress–strain curves that correspond to different level of material strength recovery. The study demonstrates the strong influence of the proportional limit of pipe material, which is associated with the onset of inelastic deformation, on the pipe collapse pressure, also noticed elsewhere. The numerical results also showed that the beneficial influence of mild heat treatment on the pipe collapse capacity is less pronounced in thinner pipes (larger value of $D/t$). Finally, selecting the fabrication factor equal to 0.93 and 1 for the bare pipe and coated pipe respectively, the DNV-ST-F101 design formulae for the calculation of collapse and propagation pressure provide conservative yet reasonable predictions when compared with the corresponding experimental and numerical results, and can be used for the mechanical design of HFW pipes in offshore pipeline applications.

## Acknowledgment

The work of the first author, Aris G. Stamou, was supported by the Hellenic Foundation for Research and Innovation (HFRI) under the 4th Call for HFRI PhD Fellowships (Fellowship Number: 9439). The authors would like to thank Corinth Pipeworks S.A., Thisvi, Greece, for funding the full-scale experimental tests at C-FER and for their permission for publishing this article. Special thanks go to Dr. Nikos Voudouris, Dr. Efthimios Dourdounis, and Dr. Athanasios Tazedakis of Corinth Pipeworks S.A. for their close cooperation throughout this research. The authors also acknowledge the valuable discussions with Dr. Konstantinos Chatziioannou on the numerical model.

## Conflict of Interest

There are no conflicts of interest.

## Data Availability Statement

The datasets generated and supporting the findings of this article are obtainable from the corresponding author upon reasonable request.

## References


[1] Kyriakides, S., and Corona, E., 2007, *Mechanics of Offshore Pipelines: Volume 1. Buckling and Collapse*, Elsevier, Oxford, UK.

[2] Kyriakides, S., and Lee, L. H., 2020, *Mechanics of Offshore Pipelines, Volume 2: Buckle Propagation and Arrest*, Gulf Professional Publishing, Oxford, UK.

[3] Karamanos, S. A., 2022, *Structural Mechanics and Design of Metal Pipes: A Systematic Approach for Onshore and Offshore Pipelines*, 1st ed., Elsevier, Amsterdam, Netherlands.

[4] Gavriilidis, I., Stamou, A. G., Palagas, C., Dourdounis, E., Voudouris, N., Tazedakis, A., and Karamanos, S. A., 2024, "Collapse Testing and Analysis of High Frequency Welded (HFW) Steel Pipes," Proceedings of the ASME 2024 15th International Pipeline Conference, Calgary, Alberta, Canada, Sept. 23–27.

[5] Gavriilidis, I., Stamou, A. G., Palagas, C., Dourdounis, E., Voudouris, N., Tazedakis, A., and Karamanos, S. A., 2024, "Heat Treatment Effects on Collapse of JCO-E Steel Pipes Under External Pressure: Experiments and Numerical Predictions," Marine Struct., **93**(1), p. 103536.

[6] Palmer, A. C., and Martin, J. H., 1975, "Buckle Propagation in Submarine Pipelines," Nature, **254**(5495), pp. 46–48.

[7] Kyriakides, S., Corona, E., and Fischer, F. J., 1991, "On the Effect of the UOE Manufacturing Process on the Collapse Pressure of Long Tubes," Offshore Technology Conference, Houston, TX, May 6–9.

[8] Herynk, M. D., Kyriakides, S., Onoufriou, A., and Yun, H. D., 2007, "Effects of the UOE/UOC Pipe Manufacturing Processes on Pipe Collapse Pressure," Int. J. Mech. Sci., **49**(5), pp. 533–553.

[9] Chatzopoulou, G., Karamanos, S. A., and Varelis, G. E., 2016, "Finite Element Analysis of UOE Manufacturing Process and Its Effect on Mechanical Behavior of Offshore Pipes," Int. J. Solids Struct., **83**, pp. 13–27.

[10] Antoniou, K., Stamou, A. G., Karamanos, S. A., Palagas, C., Tazedakis, A., and Dourdounis, E., 2023, "Finite Element Modeling of the JCO-E Line Pipe Fabrication Process; Material Properties and Collapse Pressure Prediction," Thin-Walled Struct., **192**, p. 111120.

[11] Asperheim, J. I., Das, P., Grande, B., Hömberg, D., and Petzold, T., 2024, "Numerical Simulation of High-Frequency Induction Welding in Longitudinal Welded Tubes," J. Math. Indu., **14**(1), p. 10.

[12] Kang, C., Shi, C., Liu, Z., Liu, Z., Jiang, X., Chen, S., and Ma, C., 2020, "Research on the Optimization of Welding Parameters in High-Frequency Induction Welding Pipeline," J. Manufact. Process., **59**, pp. 772–790.

[13] Techmański, Z., Stępień, J., Garstka, T., Wieczorek, P., Nowak, J., and Kobielski, A., 2023, "The Use of the Linear Energy Calculation Model in High-Frequency Induction (HFI) Tube Welding Technology to Obtain Optimal Microstructure and Weld Geometry," Metals, **13**(8), p. 1381.

[14] Techmański, Z., Stępień, J., Garstka, T., Wieczorek, P., Golański, G., and Supernak, J., 2023, "Improving the Energy Efficiency of the Production of Pipes Welded with High-Frequency Induction," Processes, **11**(9), p. 2798.

[15] Wen, B., and Pick, R. J., 1994, "Modelling of Skelp Edge Instabilities in the Roll Forming of ERW Pipe," J. Mater. Process. Technol., **41**(4), pp. 425–446.

[16] Kiuchi, M., Abe, K., and Onodera, R., 1995, "Computerized Numerical Simulation of Roll-Forming Process," CIRP Ann., **44**(1), pp. 239–242.

[17] Lee, J., Kim, D., Quagliato, L., Kang, S., and Kim, N., 2017, "Change of the Yield Stress in Roll Formed ERW Pipes Considering the Bauschinger Effect," J. Mater. Process. Technol., **244**, pp. 304–313.

[18] Han, S. W., Park, Y. C., Kang, S., Jung, S. C., and Kim, H. K., 2019, "Collapse Analysis of ERW Pipe Based on Roll-Forming and Sizing Simulations," J. Marine Sci. Eng., **7**(11), p. 410.

[19] Han, S. W., Park, Y. C., Kim, H. K., and Kang, S. C., 2020, "Effect of Strain Hardening on Increase in Collapse Pressure During the Manufacture of ERW Pipe," Appl. Sci., **10**(14), p. 5005.

[20] Tran, P.-L., Kang, S.-C., and Kim, J.-K., 2025, "Impact of Sizing Process in ERW Pipes Through Circular and Edge Forming," J. Constr. Steel Res., **229**, p. 109490.

[21] Tran, P.-L., Seong, M.-H., Kang, S.-C., and Kim, J.-K., 2026, "Analysis of Collapse Response of Offshore Pipes Under External Pressure and Bending Considering Sizing Effect," Ocean Eng., **351**, p. 124368.

[22] Det Norske Veritas, 2021, "Submarine Pipeline Systems Standard DNV-ST-F101," Høvik, Norway.

[23] Al-Sharif, A. M., and Preston, R., 1996, "Improvement in UOE Pipe Collapse Resistance by Thermal Aging," Offshore Technology Conference, Houston, TX, May 6–9.

[24] DeGeer, D., Marewski, U., Hillenbrand, H.-G., Weber, B., and Crawford, M., 2004, "Collapse Testing of Thermally Treated Line Pipe for Ultra-Deepwater Applications," Proceedings of the ASME 2004 23rd International Conference on Offshore Mechanics and Arctic Engineering, Vancouver, British Columbia, Canada, June 20–25.

[25] Timms, C., Mantovano, L., Ernst, H. A., Toscano, R., DeGeer, D., Swanek, D., de Souza, M., and Chad, L. C., 2009, "The Influence of the UOE Forming Process on Material Properties and Collapse of Deepwater Linepipe," Proceedings of the ASME 2009 28th International Conference on Offshore Mechanics and Arctic Engineering, Honolulu, HI, May 31–June 5.

[26] Arroyo, F., Solano, R. F., Mantovano, L., de Azevedo, F. B., Alves, H., Swanek, D., Silva, R., and Ernst, H., 2013, "Qualification of UOE SAWL Linepipes With Enhanced Collapse Resistance for Ultra Deepwater Applications," Proceedings of the ASME 2013 32nd International Conference on Offshore Mechanics and Arctic Engineering, Nantes, France, June 9–14.

[27] Arroyo Moreira, F., Silva, R., Mantovano, L., Solano, R., Azevedo, F., and Alves, H., 2014, "Qualification of UOE Linepipes With Enhanced Collapse Resistance," Offshore Technology Conference, Houston, TX, May 5–8, Paper No. OTC-25422-MS.

[28] Kerstens, N., Liu, P., and DeGeer, D., 2014, "Full Scale Application of Thermal Ageing in Line Pipe Material Selection for Deepwater Pipelines," Proceedings of the ASME 2014 33rd International Conference on Offshore Mechanics and Arctic Engineering, San Francisco, CA, June 8–13, OMAE2014-23869.

[29] Kathayat, T., Goyal, R. K., and Shant, J. R., 2014, "Collapse Behaviour of As-Fabricated; Thermal Aged JCOE Line Pipe - Experimental Study by External Pressure Ring Collapse Testing and FE Analysis," Offshore Technology Conference, Kuala Lumpur, Malaysia, May 25–28, Paper No. OTC-24742-MS.

[30] DeGeer, D., Timms, C., and Lobanov, V., 2005, "Blue Stream Collapse Test Program," Proceedings of the ASME 2005 24th International Conference on Offshore Mechanics and Arctic Engineering, Halkidiki, Greece, June 12–17, Paper No. OMAE2005-67260.

[31] Stahl-Eisen-Prüfblätter, 2006, *Testing and Documentation Guideline for the Experimental Determination of Mechanical Properties of Steel Sheets for CAE-Calculations SEP 1240*, Research Association for Steel Application, Wuppertal, Germany.

[32] Dassault Systèmes, 2021, *ABAQUS: Theory Manual, Version 2021*, Simulia Corporation, Providence, RI.

[33] Tassoulas, J., Katsounas, A., and Song, H.-W., 1990, "Finite Element Analysis of Propagating Buckles in Deepwater Pipelines," Offshore Technology Conference, Houston, TX, May 7–10, Paper No. OTC-6413-MS.

[34] Fu, G., Estefen, S. F., Lourenço, M., Yang, J., Paz, C. M., and Duan, M., 2021, "Buckle Propagation of Damaged SHCC Sandwich Pipes: Experimental Tests and Numerical Simulation," Marine Struct., **77**, p. 102976.

[35] Reichel, T., Pavlyk, V., Beissel, J., Kyriakides, S., and Jang, W.-Y., 2011, "New Impander Technology for Improved Collapse Resistance of Large Diameter Pipe for Deepwater Applications," Offshore Technology Conference, Houston, TX, May 2–5, Paper No. OTC-21503-MS.

[36] Toscano, R. G., Timms, C. M., Dvorkin, E. N., and DeGeer, D. D., 2003, "Determination of the Collapse and Propagation Pressure of Ultra-Deepwater Pipelines," Proceedings of the ASME 2003 22nd International Conference on Offshore Mechanics and Arctic Engineering, Cancun, Mexico, June 8–13, Paper No. OMAE2003-37339.